

## Using Multi-Walled Carbon Nanotubes as the Reducing Reagents to Prepare Pt<sub>x</sub>Sn<sub>y</sub> Composite Nanoparticles by a Pyrolysis Method for Ethanol Oxidation Reaction

Lu Liu<sup>1</sup>, JianXin Wang<sup>2</sup>, Huige Wei<sup>3</sup>, Zhanhu Guo<sup>3,\*</sup> and Keqiang Ding<sup>1,\*</sup>

<sup>1</sup>College of Chemistry and Materials Science, Hebei Normal University, Shijiazhuang 050024, P.R. China

<sup>2</sup>Fengfan Co., Ltd, Baoding, Hebei 071057, P.R. China

<sup>3</sup>Integrated Composites Laboratory (ICL), Dan F. Smith Department of Chemical Engineering, Lamar University, Beaumont, TX 77710, USA

\*E-mail: [dkeqiang@263.net](mailto:dkeqiang@263.net); [zhanhu.guo@lamar.edu](mailto:zhanhu.guo@lamar.edu)

Received: 10 December 2013 / Accepted: 18 January 2014 / Published: 2 March 2014

---

In this work, multi-walled carbon nanotubes (MWCNTs) were used as the reducing agents to prepare Pt<sub>x</sub>Sn<sub>y</sub> composite nanoparticles by a pyrolysis process, in which the nominal atomic ratios of Pt to Sn were 0.5:1, 1:1, 2:1, 2.5:1 and 3:1, respectively. X-ray diffraction (XRD), energy dispersive X-ray spectrum (EDX) and transmission electron microscopy (TEM) were utilized to feature the as prepared catalysts. Results revealed that the Pt<sub>2.5</sub>Sn<sub>1</sub> catalyst has a particle size of ~4.6 nm and a good dispersion on the surface of MWCNTs. The electrocatalytic activities of Pt<sub>x</sub>Sn<sub>y</sub>/MWCNTs towards ethanol oxidation reaction (EOR) are probed in an alkaline medium by using cyclic voltammetry (CV) and chronoamperometry (CA), indicating that Pt<sub>2.5</sub>Sn<sub>1</sub>/MWCNTs catalyst has the best electrocatalytic activity towards ethanol oxidation among the as-prepared catalysts. The reasons for the enhanced electrochemical performance on the Pt<sub>2.5</sub>Sn<sub>1</sub>/MWCNTs catalyst are also discussed.

---

**Keywords:** Nanostructures, chemical synthesis, electrochemical properties

### 1. INTRODUCTION

Due to its low toxicity, abundant availability, low permeability (but not negligible) across proton exchange membrane and higher energy density (8030 Wh kg<sup>-1</sup>) compared to that (6100 Wh kg<sup>-1</sup>) of methanol [1], the ethanol oxidation reaction (EOR) has gained much attention in the research field of direct liquid fuel cells. Although platinum (Pt) has been recognized as the most active catalyst for ethanol oxidation, the high cost and limited supply of Pt have greatly limited the development of direct

ethanol fuel cells (DEFC) [2,3]. Therefore, Pt-based composite or alloy catalysts such as binary or ternary metallic particles have been widely studied [4]. Among the developed Pt-based catalysts, the binary composite particles of Pt-Sn have been probed as one of the main promising catalysts for EOR recently. Thus, developing novel catalysts for ethanol oxidation reaction (EOR) has become a hot topic in the field of electrochemistry.

To date, there are two typical methods for synthesizing Pt-Sn nanoparticles (NPs). The first is the chemical reduction reaction. For example, Song et al. [5] described the preparation of Pt-Sn catalysts using a pulse microwave assisted polyol method, namely,  $\text{H}_2\text{PtCl}_6 \cdot 6\text{H}_2\text{O}$  and  $\text{SnCl}_2 \cdot 2\text{H}_2\text{O}$  were used as the starting materials, and ethylene glycol as the reducing agent. Sojas and co-workers [6] fabricated a carbon supported  $\text{Pt}_x\text{Sn}$  electrode, in which a commercial Pt/C catalyst and  $\text{SnEt}_4$  were used as the precursors, and the flowing  $\text{H}_2$  gas as the reducing agent. The second method is the electrochemical reduction reaction. For instance, Sun et al. [7] investigated the behaviors of irreversible adsorption of Sn adatoms on Pt (100), Pt(111) and Pt(110) electrodes using cyclic voltammetry (CV), in which the electrodes were prepared by immersing Pt single crystal electrode in a 1M  $\text{H}_2\text{SO}_4$  solution containing  $10^{-3}$  M  $\text{Sn}^{2+}$  at a fixed potential. Sieben et al. [8] investigated the oxidized carbon nanotubes supported Pt-Sn catalysts prepared by a multiple potentiostatic pulse, and found that the as-prepared bimetallic catalysts with 40 at.% Sn exhibited the highest activity for ethanol and ethylene glycol oxidation, which was attributed to the synergistic effects between the facilitation of alcohol oxidation via oxygen-containing species adsorbed on the Sn atoms, and the alteration of the electronic structure of the Pt atoms. To the best of our knowledge, the preparation of  $\text{Pd}_x\text{Sn}_y$  composite NPs via a facile pyrolysis approach in the presence of MWCNTs has not been reported.

Although many novel kinds of carbon have been developed recently [9], carbon nanotubes (CNTs) still attracted a great deal of attention due to their unique properties including high specific surface area, electrical conductivity, and good thermal and chemical stability, which make them a good catalyst support for fuel cells [10]. Thus, immobilizing metal NPs on CNTs has become an interesting field mainly due to the key roles of CNTs and metal NPs in the field of electrocatalysis, biosensors and so on [11]. To the best of our knowledge, the immobilization of  $\text{Pt}_x\text{Sn}_y$  composite NPs on CNTs via pyrolysis approach using distilled water as solvent has not been published, though we have successfully anchored platinum (Pt) NPs on the surface of multi-walled carbon nanotubes (MWCNTs) by a pyrolysis process using distilled water as the solvent [12].

Meanwhile, the electrocatalysis mechanism of Pt-Sn bimetallic catalyst towards EOR still remains unclear. For instance, Villullas' group [13] claimed that the electrocatalytic activity of the Pt-Sn/C catalysts towards ethanol oxidation is strongly influenced by the amounts of Sn in alloyed and the oxidized forms, and that the increase in the amount of alloy at the expense of oxides improves the catalytic activity. While, Sojas [6] claimed that the downward *d*-band shift of Pt in  $\text{Pt}_3\text{Sn}$  and the modification of the Pt-Pt interatomic distance by Sn incorporation could play a major role in the ethanol adsorption/oxidation process. Thus, the discrepancy on the electrocatalysis mechanism of  $\text{Pt}_x\text{Sn}_y$  catalysts toward EOR intrigued us to probe the catalyst of  $\text{Pt}_x\text{Sn}_y$  further. Also, to the best of our knowledge, all the published works on the electrocatalysis of Pt-Sn bimetallic particles were

carried out in an acid medium ( $\text{H}_2\text{SO}_4$  [14] or  $\text{HClO}_4$  [15]), and the electrocatalysis of Pt-Sn catalysts toward EOR in alkaline solution has not been reported.

In the present work, five kinds of the  $\text{Pt}_x\text{Sn}_y/\text{MWCNTs}$  based nanocomposite catalysts with various nominal atomic ratios of Pt to Sn were fabricated by a facile pyrolysis approach, in which distilled water was employed as solvent and no reducing agents were introduced. The crystalline structures and morphology of the MWCNTs supported nanoparticles were studied by XRD and TEM, respectively. The electrochemical activities of the as-prepared NPs for ethanol oxidation reaction (EOR) in alkaline medium were investigated by cyclic voltammetry (CV) and chronoamperometry, revealing that the  $\text{Pt}_{2.5}\text{Sn}_1/\text{MWCNTs}$  catalyst exhibits the highest catalytic activity among all the samples. The catalytic mechanisms of the  $\text{Pt}_{2.5}\text{Sn}_1/\text{MWCNTs}$  toward EOR were proposed.

## 2. EXPERIMENTAL

### 2.1 Materials

MWCNTs (purity > 95%) with an average diameter of 10-20 nm were purchased from Shenzhen nanotech port Co., Ltd. (China). All the electrodes were purchased from Tianjin Aida Co., Ltd (China). All the chemicals were of analytical grade and used as-received without any further treatment. Deionized water was used to prepare the aqueous solutions.

### 2.2 Preparation of $\text{Pt}_x\text{Sn}_y/\text{MWCNTs}$ nanoparticles

Firstly, 6 mL aqueous solution of  $5 \times 10^{-3}$  M  $\text{H}_2\text{PtCl}_6$  and an appropriate amount of  $\text{SnCl}_4$  were dissolved in distilled water, in which the atomic ratios of Pt to Sn were different, namely, 0.5:1, 1:1, 2:1, 2.5:1 and 3:1, respectively. Then, 10 mg MWCNTs was added to the above solution, which was ultrasonicated for 30 min. Secondly, the resultant suspension was placed in a home-made autoclave at room temperature, and then the well-sealed autoclave was transferred to a box-type furnace. Lastly, the temperature of the box-type furnace was increased to 200 °C within 30 min and maintained for 2 h to complete the pyrolysis process, which was implemented in an SRJX-8-13 box-type furnace equipped with a KSY 12-16 furnace temperature controller. After cooling down to room temperature, the filtered samples were thoroughly washed with distilled water, and dried in an ambient condition to generate the MWCNTs supported  $\text{Pt}_x\text{Sn}_y$  catalysts (denoted as  $\text{Pt}_x\text{Sn}_y/\text{MWCNTs}$ ).

### 2.3 Preparation of $\text{Pt}_x\text{Sn}_y/\text{MWCNTs}$ modified electrode

A glassy carbon (GC) electrode (geometric area of  $0.07 \text{ cm}^2$ ) was polished to a mirror finish with 50 nm alumina nanopowder suspensions before each experiment and served as a substrate for the working electrode. The working electrodes were fabricated by coating catalyst ink onto a glassy carbon electrode. The catalysts ink was prepared by dispersing 1 mg catalyst in 1 mL Nafion ethanol solution

(0.1wt%). And after ultrasonication for 20 min, about 15  $\mu\text{L}$  ink was added to the surface of the GC electrode and slowly dried in air, yielding a  $\text{Pt}_x\text{Sn}_y/\text{MWCNTs}$ -coated GC electrode.

## 2.4 Characterizations

XRD analysis of the catalyst was carried out on a Bruker D8 ADVANCE X-ray diffractometer equipped with a  $\text{Cu K}\alpha$  source ( $\lambda = 0.154 \text{ nm}$ ) at 40 kV and 30 mA. The  $2\theta$  angular region between  $10^\circ$  and  $90^\circ$  was explored at a scan rate of  $1^\circ/\text{step}$ . The particle morphology was observed by scanning electron microscopy (SEM, HITACHI, S-570) and transmission electron microscopy (TEM, HITACHI, H-7650). Energy Dispersive X-Ray Spectroscopy (EDX) spectrum analysis was carried out on X-ray energy instrument (EDAX, PV-9900, USA).

Electrochemical measurements of cyclic voltammetry (CV) and electrochemical impedance spectroscopy (EIS) were all performed on a CHI 660B electrochemical workstation (Shanghai Chenhua Apparatus, China) connected to a personal computer. EIS was performed in the frequency range from 0.05 to  $10^5 \text{ Hz}$  with an amplitude of 10 mV.

A conventional three-electrode system was employed, in which a  $\text{Pt}_x\text{Sn}_y/\text{MWCNTs}$  modified GC electrode and a platinum wire were used as the working electrode and counter electrode, respectively. The reference electrode was a saturated calomel electrode (SCE). All potentials in this paper were reported with respect to SCE. A solution of 1 M KOH containing 2 M ethanol was used to study ethanol oxidation activity. Prior to each electrochemical test, the electrolyte was bubbled with high purity nitrogen for 30 min to avoid the influence of oxygen dissolved in the electrolyte. All the experiments were carried out at room temperature.

## 3. RESULTS AND DISCUSSION

### 3.1 XRD Analysis

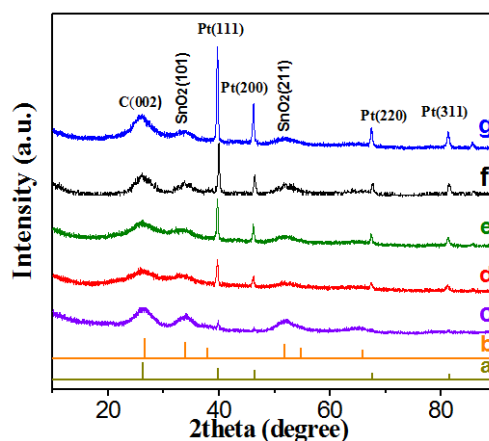


**Figure 1.** XRD patterns for the obtained samples of  $\text{Pt}_x\text{Sn}_y/\text{MWCNTs}$ . Pattern **c**:  $\text{Pt}_{0.5}\text{Sn}_1$ ; pattern **d**:  $\text{Pt}_1\text{Sn}_1$ ; pattern **e**:  $\text{Pt}_2\text{Sn}_1$ ; pattern **f**:  $\text{Pt}_{2.5}\text{Sn}_1$ ; pattern **g**:  $\text{Pt}_3\text{Sn}_1$ . Pattern **a** and **b** are the standard patterns for Pt and  $\text{SnO}_2$ .

The XRD diffraction patterns of the  $Pt_xSn_y$  catalysts are shown in Fig. 1. The small intensity peak observed in the diffraction patterns at around  $26^\circ$  can be assigned to the plane (002) of MWCNTs [12]. Except for the catalyst of  $Pt_{0.5}Sn_1$ /MWCNTs, all catalysts present a typical feature of the Pt face centered cubic (fcc) phase. The four reflections peaks at about  $40^\circ$ ,  $46^\circ$ ,  $68^\circ$  and  $82^\circ$  of  $2\theta$  values can be well associated with the Pt (111), (200), (220) and (311) planes (JCPDS 00-001-1194), respectively. Their diffraction intensity becomes weak with the addition of Sn or the increase of the Sn:Pt ratio. The shifting of diffraction peaks to a lower  $2\theta$  value was not observed, indicating that the obtained samples were not alloys of Pt with Sn [16]. The diffractogram of  $Pt_{2.5}Sn_1$ /MWCNTs catalyst shows two evident peaks at about  $34^\circ$  and  $52^\circ$ , which correspond to  $SnO_2$  (101) and (211) planes (JCPDS 00-041-1445), respectively [17]. And when the atomic ratio of Pt to Sn is 0.5:1, the intensity of diffraction peaks of Pt becomes very weak as shown by pattern c, suggesting that  $SnO_2$  was the main component in the sample of  $Pt_{0.5}Sn_1$ . Meanwhile, for all the patterns, the diffraction peak corresponding to the Pt oxides was not observed, indicating that the as-prepared samples mainly contained elementary Pt and  $SnO_2$ . The XRD patterns strongly demonstrate that the as-prepared samples have two phases except MWCNTs, this is to say, the obtained samples are composite particles rather than alloys. Probably, as reported previously [18], the catalysts containing an appropriate amount of multivalent tin oxides can provide OH species and help oxidize the adsorbed intermediates resulting from ethanol oxidation.

The average particle sizes of the catalyst were calculated from facet Pt (111) peak by the Scherrer formula [19]:

$$d(\text{\AA}) = \frac{\kappa\lambda}{\beta \cos\theta}$$

where  $\kappa$  is a coefficient (0.9),  $\lambda$  the wavelength of X-ray used ( $1.54056 \text{ \AA}$ ),  $\beta$  the full-width half maximum and  $\theta$  is the angle at position of peak maximum. The calculated particle sizes based on the plane of (111) for  $Pt_{0.5}Sn_1$ /MWCNTs,  $Pt_1Sn_1$ /MWCNTs,  $Pt_2Sn_1$ /MWCNTs,  $Pt_{2.5}Sn_1$ /MWCNTs and  $Pt_3Sn_1$ /MWCNTs are 37.44, 34.11, 33.57, 32.01 and 33.21 nm, respectively. The EDX pattern for the typical  $Pt_{2.5}Sn_1$ /MWCNTs catalyst is shown in Fig. 2. It can be seen that except for the element of C, the elements of Pt, Sn and O are all displayed clearly, indicating that the as-prepared composite samples were particles containing  $SnO_2$  and Pt rather than only Sn and Pt, which is consistent with the result shown in Fig.1.

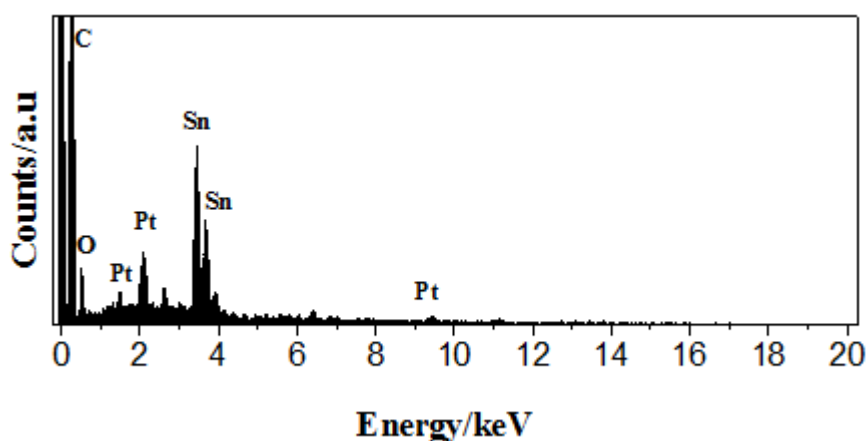
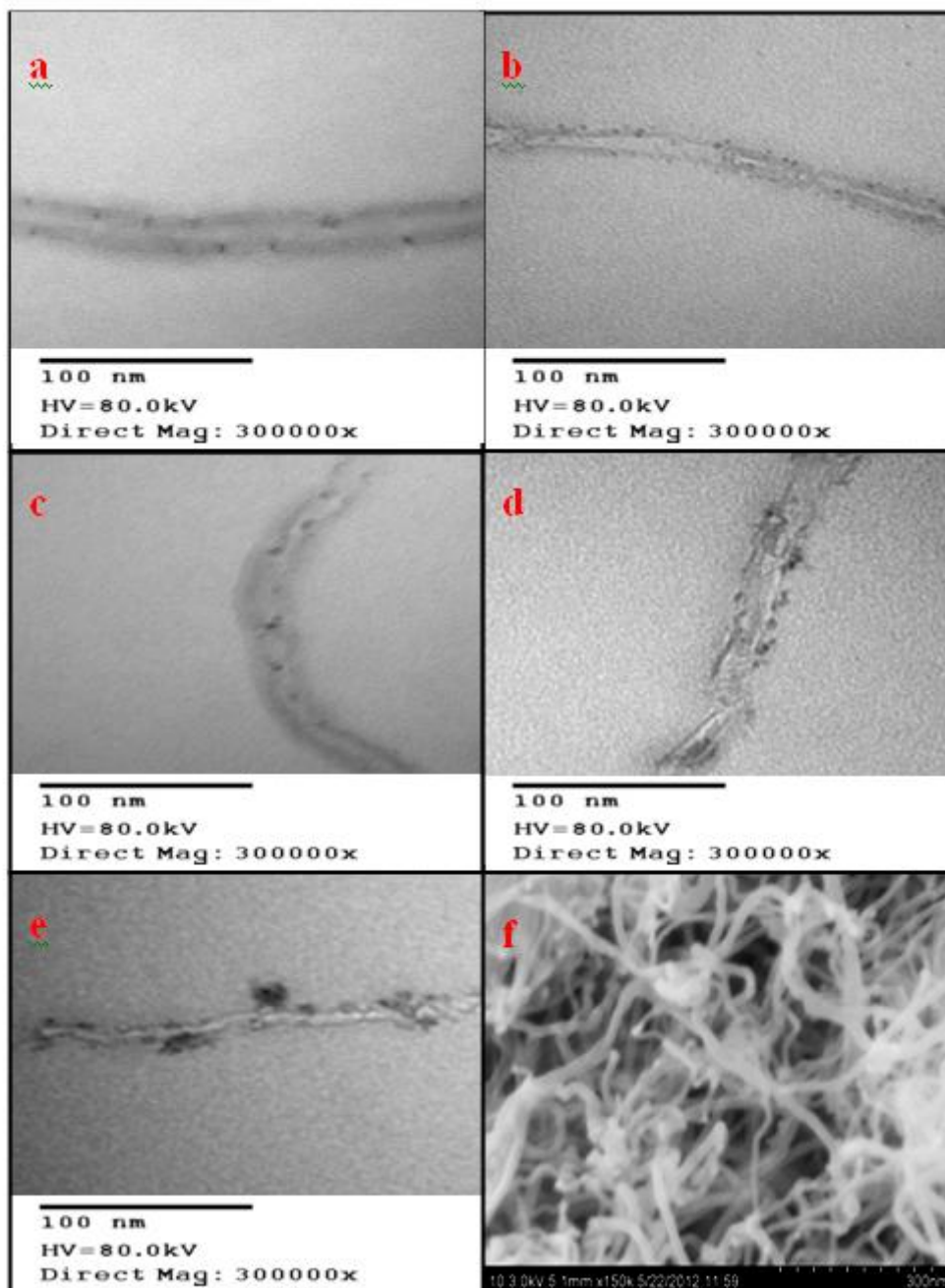


Figure 2. EDX spectrum of a typical  $Pt_{2.5}Sn_1$ /MWCNTs catalyst.

## 3.2 TEM Analysis



**Figure 3.** TEM images of (a)  $Pt_3Sn_1/MWCNTs$ , (b)  $Pt_{2.5}Sn_1/MWCNTs$ , (c)  $Pt_2Sn_1/MWCNTs$ , (d)  $Pt_1Sn_1/MWCNTs$ , (e)  $Pt_{0.5}Sn_1/MWCNTs$ . Image f is the SEM image for  $Pt_{2.5}Sn_1/MWCNTs$ .

Fig.3(f) shows the SEM image of the catalyst  $Pt_{2.5}Sn_1/MWCNT$ . After the pyrolysis process, some white dots are observed to be immobilized on the surface of MWCNTs compared to the pure MWCNTs, indicating that some substances were formed by the facile pyrolysis process. To obtain a clear observation, TEM characterizations were conducted. It is evident that for all the catalysts some black nanoparticles were anchored on the surface of MWCNTs after the pyrolysis process, Fig.3. Based on the TEM images, the particle sizes for the catalysts of  $Pt_{0.5}Sn_1$ ,  $Pt_1Sn_1$ ,  $Pt_2Sn_1$ ,  $Pt_{2.5}Sn_1$  and

Pt<sub>3</sub>Sn<sub>1</sub> are about 19.08, 12.05, 7.03, 4.60 and 6.50 nm, respectively. Thus, the catalyst of Pt<sub>2.5</sub>Sn<sub>1</sub>/MWCNTs has the smallest size among the prepared samples, corresponding to a larger surface areas compared to other catalysts when the loadings of catalysts are identical. Also, no evident aggregation of the as-prepared particles was found in the TEM images, especially for the catalyst of Pt<sub>3</sub>Sn<sub>1</sub>/MWCNTs, Pt<sub>2.5</sub>Sn<sub>1</sub>/MWCNTs, and Pt<sub>2</sub>Sn<sub>1</sub>/MWCNTs. More interestingly, when the atomic ratio of Pt to Sn was 0.5:1 (image e), cluster-shaped particles rather than spherical particles are observed. It indicates that a new substance has become into the main component of the resultant catalyst, namely, as supported by the XRD pattern c in Fig. 1, SnO<sub>2</sub> has turned into the main content of the catalyst of Pt<sub>0.5</sub>Sn<sub>1</sub>. Thus, the content of Sn in the precursors played a major role in determining the sizes and morphologies of the catalysts.

### 3.3. Electrochemical activity of Pt<sub>x</sub>Sn<sub>y</sub>/MWCNTs catalysts

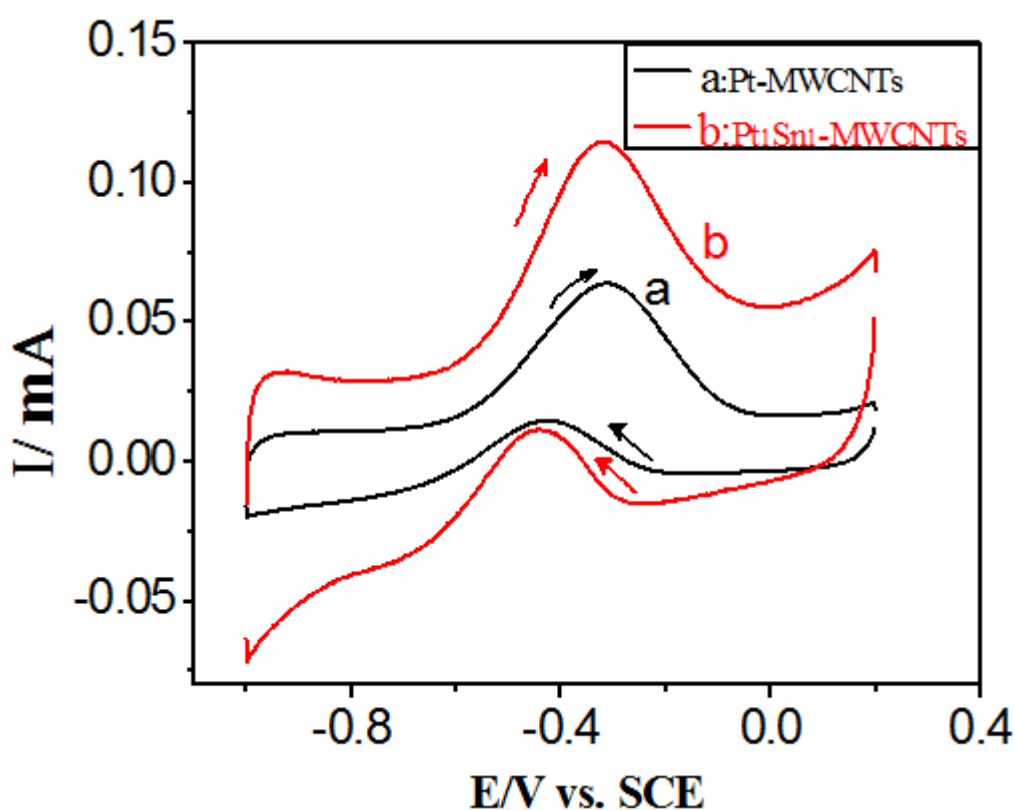


**Figure 4A.** CVs obtained on the as-prepared (a) Pt/MWCNTs and (b) Pt<sub>1</sub>Sn<sub>1</sub>/MWCNTs coated glassy carbon electrodes in a solution of 1 M KOH+2 M C<sub>2</sub>H<sub>5</sub>OH at a scan rate of 20 mVs<sup>-1</sup>

The typical cyclic voltammograms (CVs) of ethanol oxidation on the Pt<sub>1</sub>Sn<sub>1</sub>/MWCNTs catalyst synthesized by the pyrolysis method are shown in Fig. 4A. It is evident that on the pure Pt/MWCNTs coated GC electrode, a pair of well defined oxidation peaks for ethanol oxidation reaction (EOR) is clearly observed, agreeing with the former report very well [20]. And on the Pt<sub>1</sub>Sn<sub>1</sub>/MWCNTs modified GC electrode, the oxidation peak currents of EOR were significantly increased, implying that

an appropriate amount of Sn added in Pt can promote the catalytic activity of Pt toward EOR in an alkaline solution.

Nyquist plot is a typical curve in electrochemical impedance spectroscopy (EIS), which can be used for evaluating the electrochemical performance of a working electrode. Based on our previous report [21], the semicircle appearing at the high frequency region corresponds to a circuit having a resistance element parallel to a capacitance element, and a semicircle with a larger diameter corresponds to a larger charge transfer resistance. Thus, the diameter of the semicircle stands for the value of charge transfer resistance. Fig.4B describes the Nyquist plots of the EOR occurring on the Pt/MWCNTs and Pt<sub>1</sub>Sn<sub>1</sub>/MWCNTs modified GC electrodes. As shown in Fig 4B-a, a semicircle appearing in the high frequency region is followed by a nearly 45 ° line, a typical shape of Nyquist plot corresponding to an electrochemical reaction that take places at the interface between electrolyte and electrode [22].

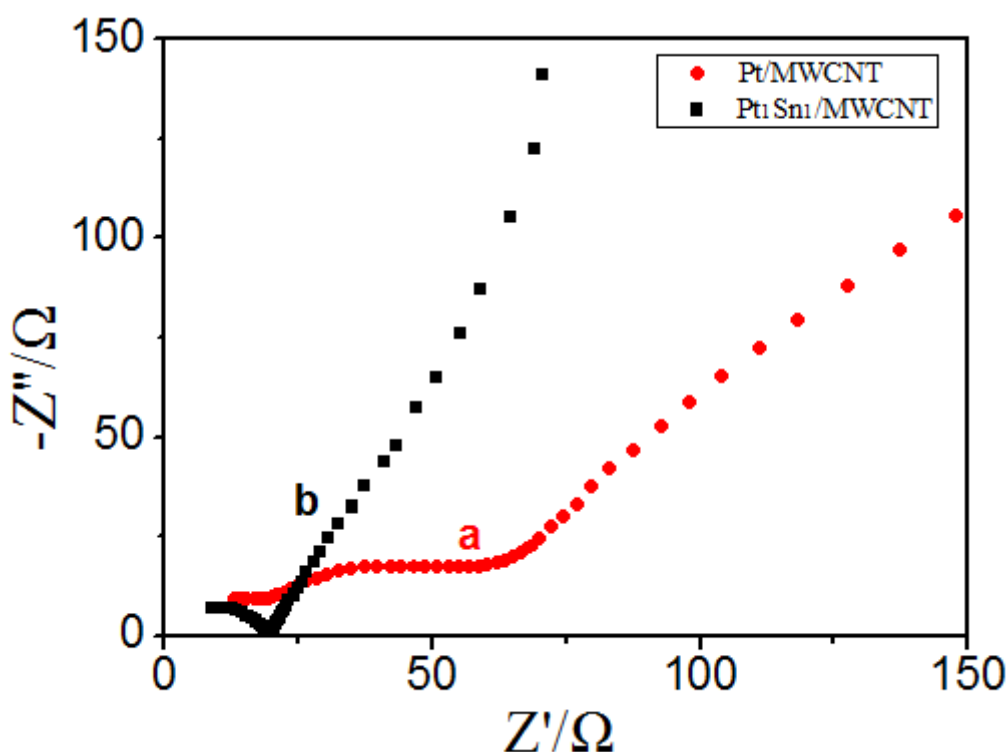


**Figure 4B.** Nyquist plot obtained on the as-prepared (a) Pt/MWCNTs and (b) Pt<sub>1</sub>Sn<sub>1</sub>/MWCNTs coated glassy carbon electrodes in a solution of 1 M KOH+2 M C<sub>2</sub>H<sub>5</sub>OH at the open circuit potential.

Interestingly, for the Pt<sub>1</sub>Sn<sub>1</sub>/MWCNTs modified GC electrode, a greatly attenuated semicircle is displayed in the high frequency region, Fig4B-b. The values of charge transfer resistance ( $R_{ct}$ ) for EOR on the catalyst of Pt<sub>1</sub>Sn<sub>1</sub>/MWCNTs and Pt/MWCNTs coated GC electrodes are estimated to be 17.5 and 52.8  $\Omega$ , respectively. Thus, the value of charge transfer resistance ( $R_{ct}$ ) for EOR on the catalyst of Pt<sub>1</sub>Sn<sub>1</sub>/MWCNTs was smaller than that on Pt/MWCNTs. It indicates that the electron

transfer process of EOR became easier relative to that on the Pt/MWCNTs modified GC electrode. In other words, the process of EOR on Pt/MWCNTs was dramatically accelerated by the addition of Sn, being consistent with the result of EOR on  $Pt_xSn_y$  coated electrode in an acidic solution [21].

The cyclic voltammograms of the ethanol oxidation on various  $Pt_xSn_y$ /MWCNTs catalysts synthesized by the pyrolysis method are shown in Fig. 5A. For the five catalysts, EOR curves can be mainly characterized by two well-defined peaks, designated as Peak **f**, centered at  $-0.31 \sim -0.24$  V in the anodic sweep, and Peak **b**, centered at  $-0.4 \sim -0.44$  V in the cathodic sweep, demonstrating that EOR can proceed on five catalysts. Generally, the oxidation peak appearing in the forward scan corresponds to the oxidation of freshly chemisorbed species coming from ethanol adsorption, and the reverse scan peak is primarily associated with the removal of carbonaceous species not completely oxidized in the forward scan [23]. The incompletely oxidized carbonaceous species, such as  $CH_3CO_{ads}$ , could accumulate on the electrode and poison the electrode. Thus, the ratio of the forward anodic peak current (peak **f**) to the reverse anodic peak current (peak **b**), i.e.,  $I_f/I_b$ , could be used to evaluate the poisoning tolerance of catalyst [24]. A larger  $I_f/I_b$  ratio indicates a better oxidation ability of ethanol during the anodic scan and less accumulation of carbonaceous residues on the electrode surface. However, as shown in Table 1, the ratio of  $I_f/I_b$  for  $Pt_{2.5}Sn_1$  is not the largest one among the obtained values though the largest peak current of EOR and the lowest onset potential in anodic sweep were exhibited by the catalyst of  $Pt_{2.5}Sn_1$ . More importantly, the electric quantity of peak **f** for the catalyst of  $Pt_{2.5}Sn_1$  was as large as 1.716 mC, which is the largest one among the obtained values. Hence, it is reasonable to think that more ethanol was electrooxidized in the anodic sweep in comparison with these cases on other catalysts.

To our knowledge, there are seldom papers considering the electric quantity consumed in the EOR when evaluating the electrocatalysis of a catalyst towards EOR. Thus, one question comes up. Is it correct or comprehensive to estimate the catalysis of a catalyst toward EOR only by the ratio of  $I_f/I_b$ ? Meanwhile, as the atomic ratio of Pt to Sn was 0.5:1, only a very weak oxidation peak in the forward direction can be observed, suggesting that the process of ethanol oxidation became very difficult on the catalyst of  $Pt_{0.5}Sn_1$  compared to those happening on the other composite nanoparticles of  $Pt_xSn_y$ . Probably, more active sites of Pt were blocked by the excess atoms of Sn or by the formed  $SnO_2$ , leading to an attenuated peak current.

**Table 1.** Electrochemical parameters obtained from Fig.5A

Catalysts	Onset potentials ( $E_{onset}$ )/V	Peak f/ $\mu$ A	Peak b/ $\mu$ A	$I_f/I_b$	Peak f electric quantity / (mC)	Peak b electric quantity / (mC)	$Q_f/Q_b$
$Pt_{0.5}Sn_1$	-0.65	7.64	0.87	8.78	0.087	0.0105	8.40
$Pt_1Sn_1$	-0.70	68.10	33.29	2.05	0.919	0.3995	2.30
$Pt_2Sn_1$	-0.66	62.18	19.85	3.13	0.862	0.2765	3.12
$Pt_{2.5}Sn_1$	-0.74	121.42	76.44	1.59	1.716	0.7015	2.45
$Pt_3Sn_1$	-0.68	82.33	65.33	1.26	1.062	0.6545	1.62

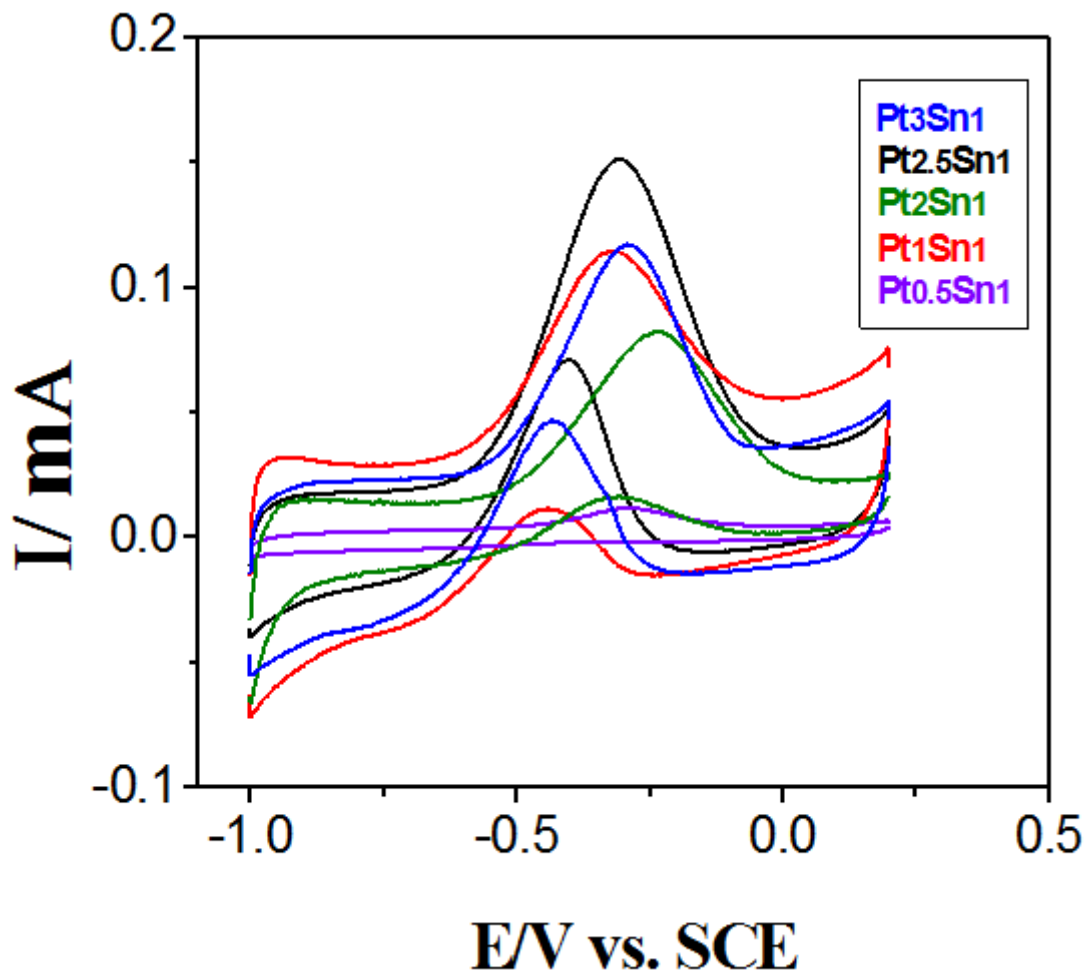


**Figure 5A.** CVs obtained on the as-prepared  $Pt_xSn_y$ /MWCNTs coated glassy carbon electrode in a solution of 1 M KOH+2 M  $C_2H_5OH$  at a scan rate of  $20 \text{ mVs}^{-1}$ .

Also, as the molar ratio of Pt to Sn is 3:1, the peak current of EOR becomes smaller as compared to that on the catalyst of  $Pt_{2.5}Sn_1$ /MWCNTs, indicating that the promoting effect of Sn for Pt would decrease when the atomic ratio of Pt to Sn was as large as 3:1. According to these electrochemical parameters summarized in Table 1 from Fig.5A, it can be deduced that the electrocatalytic activity of the  $Pt_xSn_y$ /MWCNTs catalysts towards ethanol oxidation is in the order of  $x:y=2.5:1 > 3:1 > 1:1 > 2:1 > 0.5:1$ . It substantially proved that even in an alkaline solution, an appropriate addition of Sn in the Pt/MWCNTs catalyst has good promoting effect on the ethanol oxidation, though Sn existed in the resultant catalysts in the form of  $SnO_2$ .

Nyquist plots performed on various catalysts at the open circuits are also presented in Figure 5B. It can be seen that the shape of plots for all the catalysts is similar to that of  $Pt_1Sn_1$ /MWCNTs illustrated in Fig.4B. The largest semicircle appearing in the high frequency region was displayed by the catalyst of  $Pt_{0.5}Sn_1$ /MWCNTs, indicative of a slow electron transfer process of EOR. For the catalyst of  $Pt_{0.5}Sn_1$ , the  $45^\circ$  line appearing in the lower frequency region was almost altered to be a vertical line, suggesting that the diffusion process of ethanol is different from that occurring on the other catalyst. The values of diameters for the semicircles (i.e.,  $R_{ct}$ ) appearing in the higher frequency region shown in Fig.5B are in the following increasing order, namely,  $x:y=2.5:1 < 3:1 < 1:1 < 2:1 < 0.5:1$ .

Thus, the order of the electrocatalytic activity for all the catalysts toward EOR obtained from Fig.5B is identical to that obtained from CVs shown in Fig.5A.

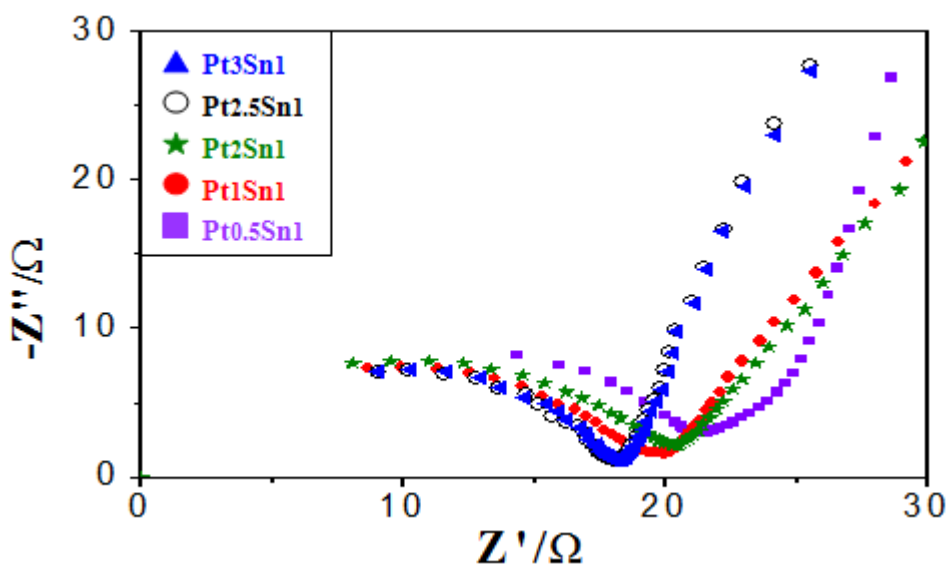


**Figure 5B.** Nyquist plots for the catalysts coated GC electrode in 1 M KOH + 2 M C<sub>2</sub>H<sub>5</sub>OH solution, in which the catalysts are different.

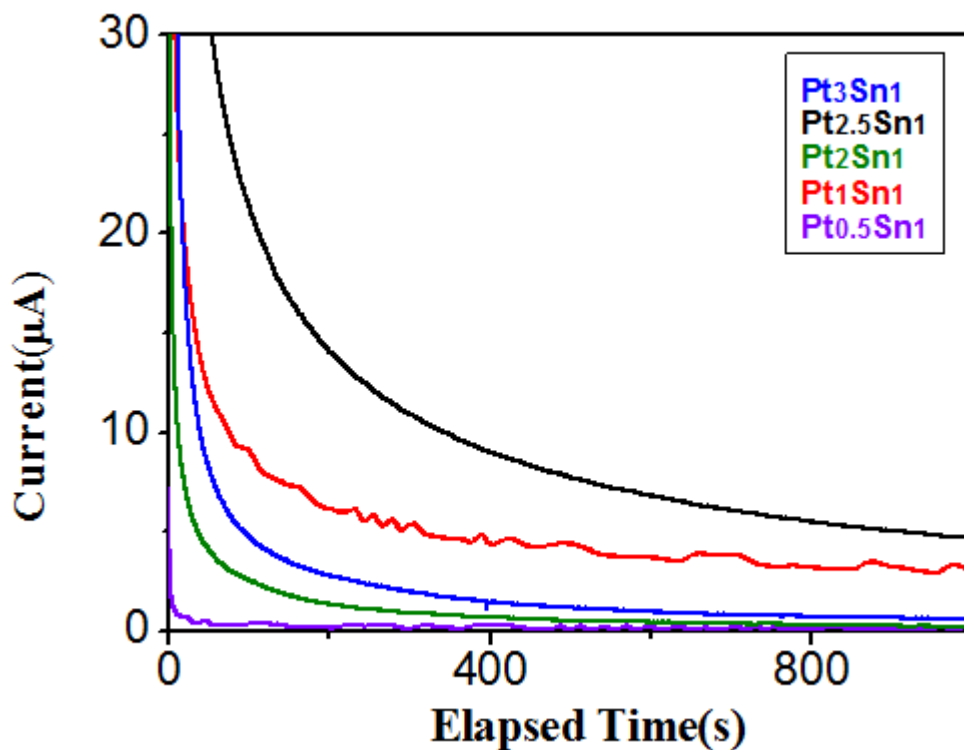


**Figure 5C.** Chronoamperometry curves of as-prepared samples-coated GC electrode in 1 M KOH + 2 M C<sub>2</sub>H<sub>5</sub>OH. The applied potential is -0.30V vs SCE.

To probe the electrochemical stability of the as-prepared catalysts for EOR, the electrochemical performance of the Pt<sub>x</sub>Sn<sub>y</sub>/MWCNTs catalysts with different Pt:Sn atomic ratios is studied by

chronoamperometry at  $-0.3$  V in  $1$  M KOH +  $2$  M  $C_2H_5OH$  solution. Their current–time curves are shown in Fig. 5C. It is found approximately that their catalytic activity for ethanol oxidation varied greatly with the Sn content. And the highest current among the samples was observed in the  $Pt_{2.5}Sn_1/MWCNTs$  catalyst. Interestingly, as the atomic ratio of Pt to Sn is  $3:1$ , instead of increasing, the polarized current decreased significantly. For the catalyst of  $Pt_{0.5}Sn_1$ , the polarized current of EOR was very small relative to those in other catalysts. It was reported that the electric conductivity of tin oxide is poor compared to Sn and Pt, which may be partially responsible for the poor electrochemical performance of EOR on the catalyst of  $Pt_{0.5}Sn_1$  due to the existence of more amount of  $SnO_2$ . Also, part of Pt active sites may be blocked by the redundant Sn or its oxides if Sn content is too high, thus it will inhibit ethanol adsorption and oxidation [18]. So the addition of Sn to Pt with only a suitable ratio can enhance the catalytic activity for ethanol oxidation in alkaline solution.

#### 3.4. Enhanced EOR by PtSn Catalysts

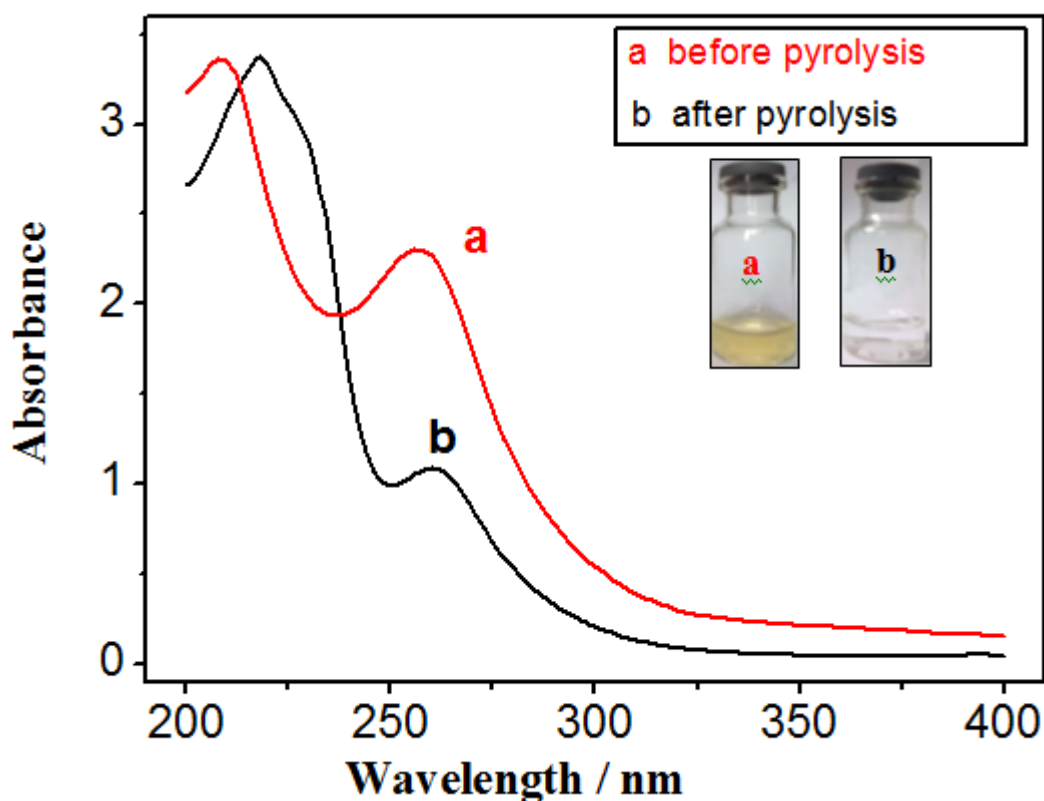


**Figure 6.** UV-vis absorption spectra of the solutions before (curve **a**) and after the pyrolysis process (curve **b**) used for preparing the catalyst of  $Pt_{2.5}Sn_1/MWCNTs$ . Photos in the inset are the solutions employed.

How do the as-prepared  $Pt_xSn_y$  nanoparticles form in this simple process of pyrolysis? The photos before and after pyrolysis for the preparation of  $Pt_{2.5}Sn_1$  are displayed by the inset of Fig. 6. It can be seen that an orange-yellow solution was prepared when the aqueous solution of  $H_2PtCl_6$  was mixed with  $SnCl_4$ . While a colorless solution was presented after pyrolysis, suggesting that all the

metal ions were reduced or changed to a new form. Fig.6 also shows the corresponding ultraviolet-visible (UV-vis) absorption spectra of the solution before and after pyrolysis process. It can be seen from curve **a** and **b** that two absorption peaks located at around 208 and 256 nm have been positioned at 217 and 261 nm after the pyrolysis process, respectively. And the prominent absorption peak at 256 nm is attributed to the absorption of  $\text{Pt}^{4+}$  ions in water [25]. Also, the intensity of the peak at 256 nm was greatly attenuated after pyrolysis, indicating that most of metal ions of Pt have been reduced. And the band at 256 nm is shifted to longer wavelength along with a decreased intensity. This shift may be attributed to the donated lone pairs of the oxygen atoms in the functional groups attached on the surface of MWCNTs to the metal ion [26], since the spectra in the far-UV region (200-250 nm) corresponds to the peptide  $n \rightarrow \pi^*$  electronic transition [27]. Probably, at a high temperature of 200 °C, most of Pt ions were reduced to pure metal by the reducing groups such as  $-\text{OH}$  and  $\text{COOH}$  attached to the surface of the MWCNTs [28].

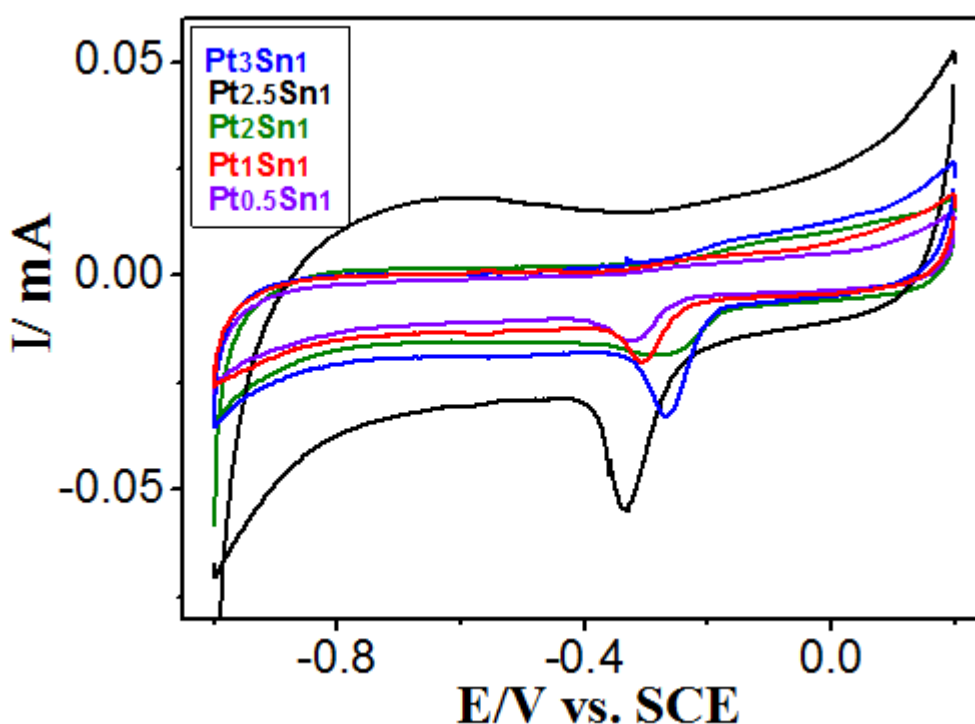
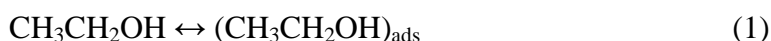


**Figure 7.** CVs obtained on the glassy carbon electrode in 1 MKOH at the scan rate of  $20 \text{ mVs}^{-1}$ . Colored curves were obtained on the  $\text{Pt}_3\text{Sn}_1/\text{MWCNTs}$ ,  $\text{Pt}_{2.5}\text{Sn}_1/\text{MWCNTs}$ ,  $\text{Pt}_2\text{Sn}_1/\text{MWCNTs}$ ,  $\text{Pt}_1\text{Sn}_1/\text{MWCNTs}$  and  $\text{Pt}_{0.5}\text{Sn}_1/\text{MWCNTs}$  modified GC electrode, respectively.

Why did the  $\text{Pt}_x\text{Sn}_y$  catalysts with various molar ratios of Pt to Sn show such different electrocatalytic activity toward EOR? To disclose the possible reasons, CVs of five catalysts in 1 M KOH are plotted in Fig.7. No evident differences of CVs were found in all the CVs. However, a close inspection revealed that there are three differences presented by the CV curve of the  $\text{Pt}_{2.5}\text{Sn}_1$  when compared to other plots of other catalysts. First, a lowered hydrogen overpotential is observed in the  $\text{Pt}_{2.5}\text{Sn}_1$  catalyst. As shown by the black curve, the peak potential of hydrogen evolution was

positively shifted for more than 80 mV in the catalyst of Pt<sub>2.5</sub>Sn<sub>1</sub> (at around -0.92 V) when compared to the other catalysts. Moreover, the peak potential of oxygen evolution in the catalyst of Pt<sub>2.5</sub>Sn<sub>1</sub> was negatively shifted for at least 60 mV as compared to other samples. That is to say, water was easily “activated” on the nanoparticles of Pt<sub>2.5</sub>Sn<sub>1</sub> in the alkaline solution when compared to the cases of other catalysts. From the obvious hydrogen evolution peaks observed in Fig.7, it can be deduced that more hydrogen gas or hydrogen atoms were formed in the vicinity of the electrode of Pt<sub>2.5</sub>Sn<sub>1</sub>. Subsequently, more ions of OH<sup>-</sup> were generated in the region close to the catalyst of Pt<sub>2.5</sub>Sn<sub>1</sub> in comparison with other kinds of Pt<sub>x</sub>Sn<sub>y</sub>. Owing to the fact that the process of EOR involves many intermediate products (such as linearly adsorbed CO and CO<sub>2</sub>, CH<sub>x,ads</sub> species [29]) and final products (such as CO<sub>2</sub>, acetaldehyde and acetic acid), its mechanism still remains unclear. However, a simplified mechanism has been provided recently as follows [30]



Thus, according to the above steps, due to the easier process of hydrogen evolution on the catalyst of Pt<sub>2.5</sub>Sn<sub>1</sub>, more ions of OH<sup>-</sup> were created yielding more amounts of OH<sub>ads</sub>. This can greatly accelerate the step (2), (3), (4) and (5). As a result, the process of EOR was significantly facilitated, leading to an enhanced peak current and lowered onset potential on the catalyst of Pt<sub>2.5</sub>Sn<sub>1</sub>.

Secondly, a larger reduction peak corresponding to the reduction of Pt oxide was observed on the catalyst of Pt<sub>2.5</sub>Sn<sub>1.5</sub>. It is generally regarded that except for the catalytic properties owned by a catalyst, the electrochemically active surface area (EASA) of the electrodes is a key parameter influencing the activity of a catalyst, thus the value of EASA was usually estimated first for analyzing the catalysis. Commonly, the value of EASA of a Pt electrode was determined by the area of the hydrogen adsorption/desorption peaks in an acid solution such as H<sub>2</sub>SO<sub>4</sub> [31]. However, in this case, only the hydrogen evolution peaks were displayed, thus, the reduction of Pt oxide can be employed to estimate the value of EASA of a Pt-based electrode approximately [32]. Therefore, the catalyst of Pt<sub>2.5</sub>Sn<sub>1</sub> has the largest value of EASA based on the previous report [32], which is consistent with the result that the catalyst of Pt<sub>2.5</sub>Sn<sub>1</sub> has the smallest particle size among the samples as shown by TEM image, Fig 3d. Thirdly, a larger rectangle-shaped CV curve is displayed by the catalyst of Pt<sub>2.5</sub>Sn<sub>1</sub>. Generally, the specific capacitance value of electrode could be evaluated directly from the following formula [33],

$$C = (I_a + I_c)/2A(dV/dt)$$

where  $I_a$ ,  $I_c$ ,  $A$  and  $dV/dt$  are the current of anodic and cathodic voltammetric curves on positive and negative sweeps, area of electrode surface and the scan rate, respectively. Thus, it can be concluded that the value of  $C$  for the catalyst of Pt<sub>2.5</sub>Sn<sub>1</sub> is due to its larger current in the potential range when assuming the area of the catalysts-modified electrodes are identical. Also, the value of double layer capacitance ( $C_d$ ) is defined as [34]:

$$C_d = \epsilon_0 \epsilon / d$$

where  $\epsilon$  is the dielectric constant of the molecules used to construct the double layer,  $\epsilon_0$  is a relative permittivity constant ( $8.68 \times 10^{-1}$ ) and  $d$  is the thickness of the double layer. Therefore, it can be inferred that the catalysts of Pt<sub>2.5</sub>Sn<sub>1</sub> with small particle size and uniform distribution have been well anchored on the surface of MWCNTs, which are immobilized on the surface of the electrode used. Thus, the value of  $\epsilon$  is greatly varied, which can probably lead to an enhanced value of  $C_d$ . In other words, the larger rectangle-shaped CV curve displayed by Pt<sub>2.5</sub>Sn<sub>1</sub> has demonstrated that the surface structure of the electrode coated by Pt<sub>2.5</sub>Sn<sub>1</sub> is rather different from those of other catalyst modified electrodes.

#### 4. CONCLUSION

For the first time, nominal Pt<sub>x</sub>Sn<sub>y</sub> composite nanoparticles with an average diameter ranging from 4 to 20 nm were prepared by a facile method of pyrolysis in the presence of MWCNTs. Analysis revealed that the smallest particle size and the presence of proper amount of SnO<sub>2</sub> may be responsible for the better electrocatalytic activity of Pt<sub>2.5</sub>Sn<sub>1</sub> toward EOR when compared to the other samples. Results from CV showed an 80 mV decrease in the onset oxidation potential and a two times enhancement in the peak current of EOR for Pt<sub>2.5</sub>Sn<sub>1</sub>/MWCNTs composite catalysts compared to that of the Pt<sub>2</sub>Sn<sub>1</sub>/MWCNTs catalysts. More importantly, CVs of the samples in alkaline medium indicated that hydrogen evolution became easier on the catalyst of Pt<sub>2.5</sub>Sn<sub>1</sub> as compared to the other catalysts, which may be partially contributed to the enhanced peak current of EOR. The present work may open a new path for the synthesis of promising electrocatalysts in the fuel cells.

#### ACKNOWLEDGEMENTS

This work was financially supported by the National Natural Science Foundation of China (No. 21173066), Natural Science Foundation of Hebei Province of China (No.B2011205014). Z. Guo acknowledges the support from US National Science Foundation (EAGER:CBET 11-37441) managed by Dr Rosemarie D. Wesson.

#### References

1. U.B. Demirci, *J. Power Sources* 169 (2007) 239-246.
2. S.Y. Shen, T.S. Zhao, J.B. Xu, *Electrochim. Acta* 55 (2010) 9179-9184.
3. N. Tian, Z.Y. Zhou, S.G. Sun, Y. Ding, Z.L. Wang, *Science* 316 (2007) 732-735.
4. N. Tian, Z.Y. Zhou, N.F. Yu, *J. Am. Chem. Soc.* 132 (2010) 7580-7581.
5. Y. Wang, S. Song, G. Andreadis, *J. Power Sources* 196 (2011) 4980-4986.
6. T. Herranz, S. García, M.V. Martínez-Huerta, *Int. J. Hydrogen Energy* 37 (2012) 7109-7118.
7. Q.W. Zheng, C.J. Fan, C.H. Zhen, *Electrochim. Acta* 53 (2008) 6081-6088.
8. J.M. Sieben, M.M.E. Duarte, *Int. J. Hydrogen Energy* 36 (2011) 3313-3321.
9. M. Xue, G. Chen, H. Yang, *J. Am. Chem. Soc.* 134 (2012) 6536-6539.
10. S. Iijima, *Nature* 354 (1991) 56-58.
11. M. Sathiyaa, A.S. Prakash, K. Ramesha, *J. Am. Chem. Soc.* 133 (2011) 16291-16299.
12. K. Ding, M. Cao, *Russ. J. Electrochem.* 44 (2008) 977-980

13. D.R.M. Godoi, J. Perez, H.M. Villullas, *J. Power Sources* 195 (2010) 3394-3401.
14. C.T. Hsieh, Y.Y. Liu, W.Y. Chen, Y.H. Hsieh, *Int. J. Hydrogen Energy* 36 (2011) 15766-15774.
15. S. García-Rodríguez, M.A. Peña, J.L.G Fierro, *J. Power Sources* 195 (2010) 5564-5572.
16. L. Li, M. Huang, J. Liu, Y. Guo, *J. Power Sources* 196 (2011) 1090-1096.
17. Z. Liu, B. Guo, L. Hong, *Electrochem. Commun.* 8 (2006) 83-90.
18. M. Zhu, G. Sun, Q. Xin, *Electrochim. Acta* 54 (2009) 1511-1518.
19. V. Radmilovic, H.A. Gasteiger, P.N. Ross, *J. Catal.* 154 (1995) 98-106.
20. E. Higuchi, K. Miyata, T. Takase, *J. Power Sources* 196 (2011) 1730-1737.
21. K. Ding, Z. Jia, Q. Wang, *J. Electroanal. Chem.* 513 (2001) 67-71.
22. K. Ding, G. Yang, S. Wei, P. Mavinakuli, Z. Guo, *Ind. Eng. Chem. Res.* 49 (2010) 11415-11420.
23. R.N. Singh, A. Singh, Anindita, *Int. J. Hydrogen Energy* 34 (2009) 2052-2057.
24. G.Y. Zhao, C.L. Xu, D.J. Guo, H. Li, H.L. Li, *J. Power Sources* 162 (2006) 492-496.
25. T. Teranishi, M. Hosoe, T. Tanaka, M. Miyake, *J. Phys. Chem. B* 103 (1999) 3818-3827.
26. M. Asadi, Z. Asadi, S. Torabi, N. Lotfi, *Spectrochim. Acta Part A* 94 (2012) 372-377.
27. X. Wu, P. Du, P. Wu, C. Cai, *Electrochim. Acta* 54 (2008) 738-743.
28. D. Hulicova-Jurcakova, M. Seredych, G.Q. Lu, N.K.A.C. Kodiweera, P.E. Stallworth, S. Greenbaum, T.J. Bandosz, *Carbon* 47 (2009) 1576-1584.
29. H. Wang, Z. Jusys, R.J. Behm, *J. Power Sources* 154 (2006) 351-359.
30. Z.X. Liang, T.S. Zhao, J.B. Xu, L.D. Zhu, *Electrochim. Acta* 54 (2009) 2203-2208.
31. B. Habibi, N. Delnavaz, *Int. J. Hydrogen Energy* 36 (2011) 9581-9590.
32. S.J. Xia, V.I. Birss, *Electrochim. Acta* 45 (2000) 3659-3673.
33. J.N. Broughton, M.J. Brett, *Electrochim. Acta* 50 (2005) 4814-4819.
34. V. Suryanarayanan, S. Yoshihara, T. Shirakashi, *Electrochim. Acta* 51 (2005) 991-999.